Magnetic properties and Mn mixed valence in $Bi_2Sr_2MnO_{6+x}$ and $BiPbSr_2MnO_6$

1997 J. Phys.: Condens. Matter 9 3931

(http://iopscience.iop.org/0953-8984/9/19/013)

J. Phys.: Condens. Matter **9** (1997) 3931–3941. Printed in the UK PII: S0953-8984(97)75651-0

Magnetic properties and Mn mixed valence in $Bi_2Sr_2MnO_{6+x}$ and $BiPbSr_2MnO_6$

C B Azzoni†, M Catti‡, A Paleari§ and C Pogliani§

† Istituto Nazionale Fisica della Materia–Dipartimento di Fisica 'Alessandro Volta', Universitá di Pavia, via Bassi 6, I-27100 Pavia, Italy

‡ Dipartimento di Chimica Fisica ed Elettrochimica, Universitá di Milano, via Golgi 19, I-20133 Milano, Italy

§ Istituto Nazionale Fisica della Materia–Dipartimento di Fisica, Universitá di Milano, via Celoria 16, I-20133 Milano, Italy

Received 24 June 1996, in final form 27 January 1997

Abstract. Electron paramagnetic resonance (EPR) and static magnetic susceptibility data have been collected on a set of powder samples of $Bi_2Sr_2MnO_{6+x}$ and $BiPbSr_2MnO_6$, Mn analogues of one-layer BSCCO superconductors. EPR spectra, analysed in a crystal field approach, indicate that typically 40–50% of Mn^{3+} ions are substituted by Mn^{2+} species in the lead-free compound and that strong deviations of the average Mn oxidation state can be introduced by reduced thermal cycles during the preparation procedure, as supported by XPS analysis. Susceptibility data, compared with the EPR response, suggest that Mn mixed valence may be a crucial factor, together with structural modulations or local anisotropy, in determining the variety of magnetic behaviours (mainly antiferromagnetic and metamagnetic) observed in these compounds.

1. Introduction

In the Bi–Sr–Ca–Cu–O family of high-T_c superconductors, the number of adjacent CuO_2 planes, as well as the distortions connected with oxygen or cation nonstoichiometry and cation doping (e.g. Pb in the BiO layers), affect the superconductive [1] as well as the magnetic properties [2, 3]. Several studies were carried out on related non-superconductive compounds, with partial or complete substitution of Cu by other metal ions [6, 7], giving insight into a few aspects of the magnetic interactions and relating them to the structural properties. The structural modulation which gives rise to incommensurate superstructure in bismuth cuprates [4, 5], now definitely associated with extra oxygen in the Bi layers, was successfully investigated in Fe-, Co- and Mn-substituted compounds in connection with the observed magnetic phases [8–13]. In particular, $Bi_2Sr_2MnO_{6+x}$ and $BiPbSr_2MnO_6$ showed different magnetic behaviours related to the presence, in the former, and the lack, in the latter, of the structural modulation [10, 13]. Antiferromagnetic features with field-induced transition to ferrimagnetic phases (metamagnetism) appear from results on $Bi_2Sr_2MnO_{6+x}$ single crystals [10]. In this compound, the spin direction as well as the field-induced ferrimagnetic moment were determined to be along the c axis. By contrast, $BiPbSr_2MnO_6$ [13] seems to behave as a canted antiferromagnet with weak ferromagnetic moment in the layer.

However, a few aspects are not yet understood in the magnetism of these layered bismuth manganites, and a comparison with the analogous compounds with Sr substituted by Ca gave

0953-8984/97/193931+11$19.50

somewhat puzzling results [10]. Furthermore, some peculiar features of the $BiPbSr_2MnO_6$ single-crystal behaviour turned out to be different in powder samples, particularly the magnetic transition temperature [13]. The spin value is also somewhat uncertain, as the susceptibility data give a mean magnetic moment slightly larger than that expected for Mn^{3+} ions with $S = 2$ [10]. The origin of this fact was not analysed and it is not clear whether it really reflects the presence of different Mn valence states, as can be surmised from x-ray absorption spectroscopy results [11]: these show effective Mn oxidation states of $+2.6$ and $+2.9$ in $Bi_2Sr_2MnO_{6+x}$ and $BiPbSr_2MnO_6$, respectively.

In order to contribute to the clarification of these points, we carried out magnetic measurements on a set of $BiPbSr_2MnO_6$ and $Bi_2Sr_2MnO_{6+x}$ powder samples, checking the consistency of our data with the reported results on single crystals and the existence of possible effects of deviations from the stoichiometry. Electron paramagnetic resonance (EPR) measurements were also performed, looking for possible resonances from Mn ions: any investigation of this type on these compounds was still lacking, to our knowledge, although from the EPR response some indication may be obtained about the valence and spin state of the Mn ions. From these results, the role of the structural features and of possible deviations from the formal Mn valence state on the magnetic properties of $Bi_2Sr_2MnO_{6+x}$ and $BiPbSr_2MnO_6$ will be discussed.

2. Experimental details

Powder samples of $Bi_2Sr_2MnO_{6+x}$ and $BiPbSr_2MnO_6$ were prepared by a standard solid state reaction in platinum boats [11]. The appropriate amounts of Bi_2O_3, PbO and $SrCO_3$ commercial powders (analytical grade) were mixed in stoichiometric ratios, with Mn_2O_3 obtained by heating MnO_2 in air at 750 °C for 15 h. The mixture was first heated slowly to 800 °C and kept at this temperature for 15 h. The powder obtained was ground and fired in two cycles of 20 h, first at 900 °C then at 950 °C, and finally furnace cooled to room temperature. After each firing cycle, samples were powdered and pelletized. All heating, firing and cooling were carried out in an argon flow in order to avoid oxidation of Mn^{3+}. Samples A and B of table 1 were prepared in this way. In other instances, the two final thermal treatments at 900 and 950 °C were carried out in separate steps with intermediate physical characterization (sample C and D of table 1). The effective Mn oxidation state of lead-free samples was controlled by x-ray photoelectron spectroscopy (XPS). XPS spectra were collected by using an M-Probe Surface Science spectrometer employing monochromatized Al Kα radiation with an energy resolution of 0.6 eV. In figure 1 two representative XPS spectra are shown together with the numerical fits obtained by using MnO and Mn_2O_3 reference data. The results of the analysis are reported in the last column of table 1. The purity and the lattice features of the phases were checked by x-ray diffraction measurements with a Siemens D500 diffractometer (Cu Kα radiation).

Static magnetic susceptibility measurements were carried out from 300 down to 77 K, in magnetic fields ranging from 0.01 to 0.45 T, using a Faraday balance susceptometer. The final accuracy of the mass susceptibility data results in an error of a few per cent. The magnetic field dependence of the magnetization was analysed by changing the field intensity at fixed temperature or by comparing magnetization–temperature curves at different magnetic fields in the case of magnetically ordered phases. A careful calibration of the temperature scale with a paramagnetic standard gave a final reliability of the sample temperature of ± 1 K.

EPR spectra were collected in the temperature range 120–400 K by a Bruker spectrometer at 9.12 GHz. Particular care was taken with the reproducibility of the sample

Table 1. Type of magnetic behaviour, effective magnetic moment (in Bohr magnetons) from χ data, fractions of EPR-active Mn sites (in brackets, the resulting average Mn oxidation state) and average oxidation state from XPS data for the samples studied.

Sample	Nominal composition	Magnetism[a]	μ_{eff}	x_{EPR}	XPS data
A	$BiPbSr_2MnO_6$	AF	—	0.06 (2.9)	—
B	$Bi_2Sr_2MnO_{6+x}$	F	5.3	0.5 (2.5)	2.64
C[b]	$Bi_2Sr_2MnO_{6+x}$	P	5.5	0.9 (2.1)	2.00
D	$Bi_2Sr_2MnO_{6+x}$	AF	—	0.3 (2.7)	2.67

[a] AF, antiferromagnetic behaviour; F, field-induced ferrimagnetism; P, prevalent paramagnetism.
[b] Sample obtained after only two thermal cycles instead of three; a further thermal treatment, carried out after 2 months, has transformed it into sample D.

positioning in the resonant cavity and of the sample amount, in order to avoid modifications of the Q factor of the microwave cavity. The EPR centre concentrations were then estimated from the experimental signal areas, calculated by double integration of the first-derivative signal, and rescaled according to the signal of a paramagnetic standard. Owing to the very broad lineshapes, extending to magnetic field values higher than the experimental limit, this type of calculation may be affected by a significant error. However, the first decimal figure of the concentration of EPR centres (table 1) can be considered to be fully reliable.

3. Results

3.1. Susceptibility data

The temperature dependence of the mass susceptibility χ_m of $BiPbSr_2MnO_6$, corrected for core diamagnetism (-1.11×10^{-6} cm^3 g^{-1} [14]), is reported in figure 2. A narrow peak (about 2 K wide) is observed in the χ_m curve at 195 ± 1 K. Below this peak, χ_m slowly decreases and no remanent magnetization is observed such as that reported for single crystals [10]. Indeed, χ_m does not depend on the applied field throughout the temperature range investigated, showing that the magnetization–magnetic field behaviour is linear down to the lowest temperature. Between 195 and 300 K, χ_m does not follow any Curie–Weiss behaviour but just increases slowly. Detailed measurements of the 195 K peak at different magnetic fields, on both heating and cooling, are reported in the inset of figure 2: no magnetic field dependence is observed.

Figure 3 shows χ_m data of $Bi_2Sr_2MnO_{6+x}$ as a function of temperature; measurements on samples prepared by different thermal treatments are compared. Samples undergoing a complete thermal cycle (see curve B) show a Curie–Weiss behaviour at least down to 150 K, and pronounced transition features at $T_N \approx 125$ K. The paramagnetic data, corrected for core diamagnetism, may be interpolated by the Curie–Weiss expression $N\mu^2/[3k_B(T+\theta)]$ (where N is the number of paramagnetic ions per mass unit and k_B the Boltzmann constant): an effective magnetic moment μ_{eff} per manganese ion, in Bohr magnetons, of about $5.3 \pm 0.1\mu_B$ is obtained in these cases (sample B in table 1). An abrupt change of χ_m is observed in samples of type B at $T_N = 125$ K, a peak about 10 K wide being present in the χ_m curve, in accordance with results reported by others for single crystals [10]. Below T_N, these samples show magnetic behaviours against temperature which depend on the cycle of applied magnetic field (see figure 4 for sample B of table 1), as already observed [10]. Actually our results (at magnetic field values lower than 0.5 T) do not show the extreme behaviour observed in [10] where the peak was no longer observed owing to the

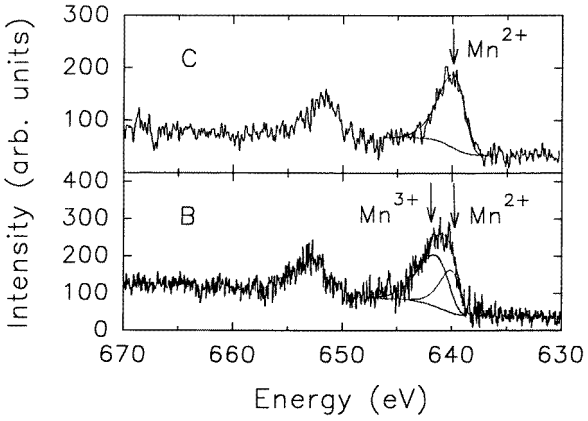

Figure 1. XPS spectra of $Bi_2Sr_2MnO_{6+x}$ showing the coexistence of Mn^{3+} and Mn^{2+} in samples prepared after a complete thermal cycle (sample B) and the presence of Mn^{2+} alone in samples prepared with reduced thermal treatments (sample C). The components of the fits are also shown together with the baseline corrections.

monotonic increase of χ_m around T_N. Nevertheless, the peak appears broadened on the low-temperature side on increasing the applied magnetic field (figure 4(a)), indicating the field-induced increase of the magnetic moment. Measurements made on heating reproduce the behaviour observed on cooling (figure 4(a)) only after a cooling cycle in applied magnetic field; by contrast, data collected on heating after zero-field cooling or by switching off the field at low temperature (figure 4(b)) show a less pronounced increase of χ_m below T_N. These are typical metamagnetic features consisting of the presence of a field-induced transition between different magnetic phases, with critical magnetic field values of the order of 10^{-1}–10^{0} T.

By contrast, samples prepared with reduced thermal cycle (such as sample C in table 1) remain substantially paramagnetic down to the lowest temperature investigated. Other $Bi_2Sr_2MnO_{6+x}$ samples (such as sample D, obtained by completing the thermal treatment of sample C, which possesses a slightly higher Mn oxidation state with respect to sample B) show AF-like magnetic behaviour with χ_m decreasing below T_N (curve D in figure 3), similar to the behaviour observed for $BiPbSr_2MnO_6$. In table 1, we report the types of magnetic behaviour observed in the representative samples.

3.2. EPR spectra

All the investigated samples show intense EPR responses consisting of very broad signals arising from large densities of paramagnetic centres. The lineshapes of these signals are very complex and sample dependent, probably owing to strong dipolar and magnetic interactions varying from sample to sample. In figure 5 we report the spectrum observed for $BiPbSr_2MnO_6$ (sample A of table 1) together with some representative spectra of $Bi_2Sr_2MnO_{6+x}$ samples (the metamagnetic sample B, the paramagnetic sample C and the AF sample D). The EPR spectrum of stoichiometric $BiPbSr_2MnO_6$ is a signal with g_{eff} slightly less than two and linewidth of 80 mT at room temperature. This signal does not show any drastic change from 290 K down to temperatures below the peak in the χ_m curve, apart a slight decrease of its intensity (figure 6(a)) that follows the decrease of χ_m. By

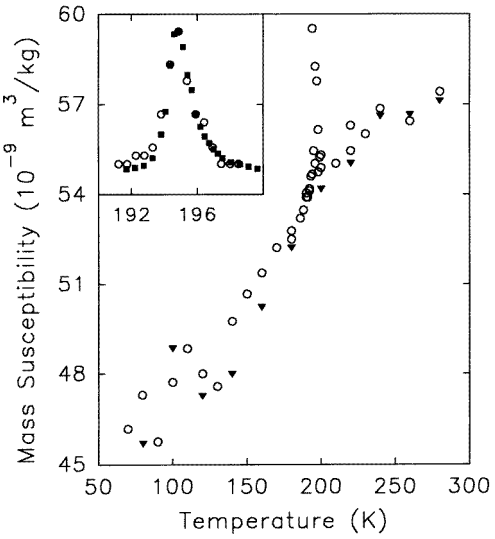

Figure 2. Mass susceptibility χ_m against temperature in $BiPbSr_2MnO_6$, at 200 mT (circles) and from magnetization measurements (triangles). In the inset, data are reported for a restricted temperature range around the transition temperature, at 100 mT (squares) and 400 mT (circles).

contrast, in $Bi_2Sr_2MnO_{6+x}$ the EPR signals are generally broader (about 300–400 mT). In samples possessing metamagnetic properties (sample B), a strong temperature dependence is observed (figure 6(b)): the signal broadens and shifts on lowering the temperature and finally disappears below the magnetic transition temperature. Intense signals are detected in $Bi_2Sr_2MnO_{6+x}$ samples with a nearly paramagnetic behaviour (sample C). In these cases the signal generally is weakly influenced by the temperature.

Finally, we note that the EPR centre density appears to be larger in samples with higher effective magnetic moment χ_{eff} per Mn ion from susceptibility data (table 1). The order of magnitude of the estimated spin densities is very large (10^{20} g^{-1}) in all $Bi_2Sr_2MnO_{6+x}$ samples, where the ideal density of Mn sites is 8.1×10^{20} g^{-1}. The density in stoichiometric $BiPbSr_2MnO_6$ is instead smaller by an order of magnitude with respect to the lowest density in the other samples.

4. Discussion

By comparing results obtained from differently prepared samples of $Bi_2Sr_2MnO_{6+x}$, the magnetic properties appear to be strongly affected by the sequence of thermal treatments. Thus the oxygen content x, and the related oxidation state of Mn, are the crucial parameters. Indeed, a wide variety of magnetic behaviours are observed within a set of samples showing comparable x-ray diffraction patterns but different Mn oxidation state, as indicated by XPS data (see table 1). Care should therefore be taken in ascribing a specific magnetic response to bare structural features of these compounds. In particular, the real origin of the in-plane ferrimagnetic moment observed in $Bi_2Sr_2MnO_{6+x}$ single crystals [10] has to be examined. In the following we analyse the EPR data, showing that they suggest the coexistence of different manganese valence states with very different degrees of spin isotropy. Then their role in the magnetic susceptibility behaviour is discussed.

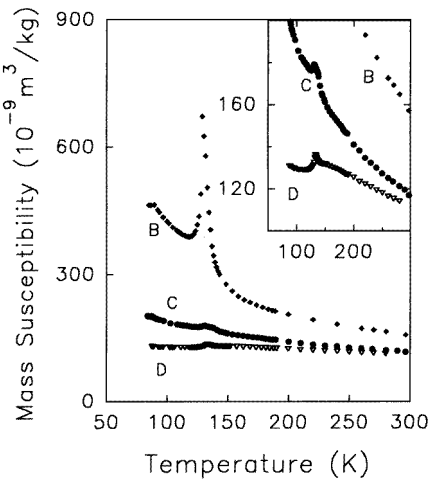

Figure 3. Mass susceptibility against temperature in $Bi_2Sr_2MnO_{6+x}$ powder samples prepared in different conditions. In the inset, low-χ_m data are reported on an enlarged scale. All curves are labelled according to table 1.

4.1. EPR data

The order of magnitude of the concentrations of paramagnetic centres estimated in the samples characterized by the most intense EPR signals (about 10^{20} g^{-1}) is consistent with stoichiometric density values of manganese paramagnetic ions: thus, assignments to impurities or spurious phases are ruled out. On the other hand, the spread of estimated density values of EPR centres indicates that not all Mn sites in the lattices of $BiPbSr_2MnO_6$ and $Bi_2Sr_2MnO_{6+x}$ are EPR active, but only a fraction, probably ranging from a few per cent up to more than 50%.

Mn^{2+}, Mn^{3+} and Mn^{4+} ions are the paramagnetic ions possibly responsible for the observed EPR spectra. Indeed, Mn^{4+} ions should not be present in significant amounts, since just a few per cent would involve too large an oxygen surplus for the lattice, and detectable spurious phases should be revealed in the diffraction pattern, so, we are only concerned with Mn^{3+} and Mn^{2+} ions. Both high-spin (HS) and low-spin (LS) electronic configurations are in principle possible for octahedrally coordinated Mn^{3+} and Mn^{2+} ions ($S = 2$ and $S = 1$ for d^4 Mn^{3+}, $S = \frac{5}{2}$ and $S = \frac{1}{2}$ for d^5 Mn^{2+}), although HS states are usually strongly preferred. Indeed, the latter configurations are fully consistent with the effective magnetic moments per ion derived from susceptibility data. The calculated spin only values of the magnetic moment $\mu = g[S(S+1)]^{1/2}\mu_B$ in HS configurations are 5.9 and $4.9\mu_B$ for Mn^{2+} and Mn^{3+}, respectively, comparing well with the μ_{eff} experimental values ranging between 5.2 and $5.5\mu_B$. For LS configurations, by contrast, $\mu = 1.7$ and $2.8\mu_B$ would be expected for Mn^{2+} and Mn^{3+}, respectively.

The EPR response of HS Mn^{2+} in octahedral environments is well known [15] and is characterized by $\Delta m_S = \pm 1$ transitions within the $S = \frac{5}{2}$ multiplet of levels, and by hyperfine structure (hfs) from interactions with the nuclear spin $I = \frac{5}{2}$. In distorted environments causing anisotropic zero-field splittings of the multiplet, transitions within the $m_S = \pm\frac{1}{2}$ doublet dominate the spectrum in polycrystalline samples, because the intensity of transitions to higher-spin states is quenched by the strong angular dependence of the corresponding spectra. The resulting EPR response consists of signals with $g \approx 2$ with

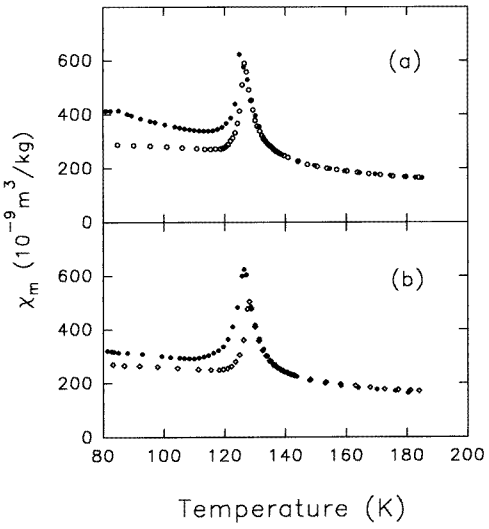

Figure 4. Mass susceptibility against temperature in a metamagnetic $Bi_2Sr_2MnO_{6+x}$ sample (sample B of table 1) measured at 0.2 T (open circles) and 0.4 T (filled circles) (a) by cooling in applied magnetic field and (b) by heating after zero-field cooling.

large asymmetric broadening from anisotropic transitions to higher-spin states and from unresolved hyperfine structure.

The EPR spectrum of Mn^{3+} ions was rarely observed [15, 16] and this precludes a reliable assignment from a simple comparison. Therefore, in order to determine the expected EPR response from Mn^{3+} ions in the investigated materials, we calculated the energy level structure of Mn^{3+} ions in the crystal field pertaining to the known coordination geometry of Mn in these layered structures. We calculated *ab initio* the electrostatic potential $V(\boldsymbol{r}) = \sum q_j/4\pi\varepsilon_0|(\boldsymbol{R}_j - \boldsymbol{r})|$ due to the charges q_j in the positions $\boldsymbol{R}_j$ of the surrounding ions, by starting from the neutron diffraction data [12] and by expanding the potential in Legendre polynomials and Stevens operators [17]. Then, the eigenstates and the eigenvalues of the Mn^{3+} ion were calculated by diagonalizing the 25×25 matrix obtained from the Hamiltonian $\mathcal{H} = \mathcal{H}_{cf} + \mathcal{H}_{so} = -|e|V(\boldsymbol{r}) + \lambda \boldsymbol{L} \cdot \boldsymbol{S}$ (with spin–orbit coupling constant $\lambda = 60$ cm^{-1} [16]) operating on the basis $|L, M_L, S, M_S\rangle$ of the ^{5}D 3d^4 Mn^{3+} ion. The g tensor is obtained by applying the Zeeman Hamiltonian $\mathcal{H}_Z = \mu_B(\boldsymbol{L} + 2\boldsymbol{S}) \cdot \boldsymbol{B}$ to the low-lying energy levels.

In figure 7 the calculated energy splittings of the ground state are reported as a function of the magnetic field B, with B along the c axis or perpendicular to it. These results, consistent with those previously found from a phenomenological analysis of the EPR signal of substitutional Mn^{3+} in TiO_2 [16], clarify the spin dimensionality of Mn^{3+} in these layered oxides. In fact, one may note that the Mn^{3+} ion turns out to be strongly anisotropic, giving rise to a non-null magnetic moment only along the direction orthogonal to the oxide layers. This calculation matches with previous neutron diffraction analysis [10] and suggests a two-dimensional Ising model to analyse the magnetism of this system. On the other hand, the fine and Zeeman splittings shown in figure 7 rule out the attribution of the observed EPR signal to Mn^{3+} ions. In fact, the fine splitting among the $m_S = \pm 2$, the $m_S = \pm 1$ and the $m_S = 0$ energy levels is almost two orders of magnitude larger than the photon energy (about 4×10^{-2} meV) in our X-band EPR measurements, precluding the observation

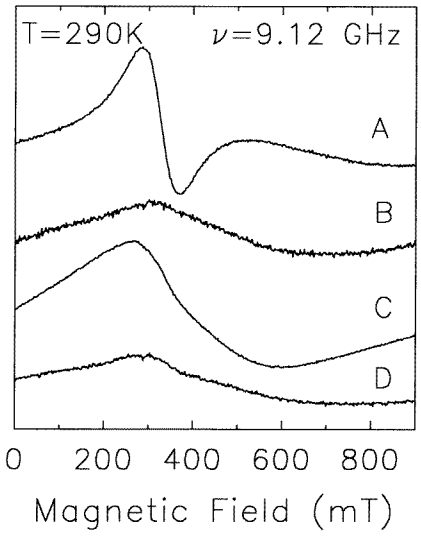

Figure 5. The EPR first-derivative X-band spectrum at 290 K of $BiPbSr_2MnO_6$ and $Bi_2Sr_2MnO_{6+x}$ powder samples labelled as in table 1. The signals are normalized to the same sample mass and spectrometer sensitivity.

of $\Delta m_S = \pm 1$ magnetic dipole transitions. In summary, this analysis suggests the lack of detectable signal from Mn^{3+} ions and attributes to these sites a strong magnetic anisotropy. On the other hand, the features of the experimental signals point to the presence of nearly isotropic ions, as Mn^{2+} in substitutional octrahedral positions. Therefore, the x_{EPR} values appearing in table 1 correspond to direct estimates of the fractions of Mn^{2+} ions over the $Mn^{2+} + Mn^{3+}$ sum, allowing also one to derive average values of the Mn oxidation states (see table 1). These compare well with the valence state obtained by x-ray absorption spectroscopy [11] (except for sample C which underwent an incomplete thermal treatment) and are in good agreement with the values from XPS measurements (last column of table 1).

4.2. Susceptibility data

The analysis of the EPR data suggests we carefully re-consider the real origin of the net in-plane magnetic moment in the ordered phases of $Bi_2Sr_2MnO_{6+x}$ and $BiPbSr_2MnO_6$. In particular, for $Bi_2Sr_2MnO_{6+x}$, the coexistence of Mn^{3+} and Mn^{2+} ions should be taken into account in addition to the slight differentiation of sites arising from the modulated structure observed by diffraction techniques. Indeed, an indication of significant spin differences from site to site arose from mean-field calculations of the expected width of the low-field susceptibility peak observed at T_N in $Bi_2Sr_2MnO_{6+x}$ [10]: fluctuations were invoked since reasonable small differences between spins of the same cationic species in non-equivalent sites of the modulated structure did not account for the experimental width of the peak. More consistent spin differences may instead arise from the presence of a relevant fraction of Mn^{2+} ions. These may cause uncompensated magnetic moments in the ordered phase, i.e. ferrimagnetism within each layer, if Mn^{2+} ions are associated with specific structural sites of the observed modulation. Therefore, we believe that the effects of different spin states arising from the coexistence of Mn^{3+} and Mn^{2+} should be carefully considered.

The values of the μ_{eff} magnetic moment from the χ_m data may be usefully compared

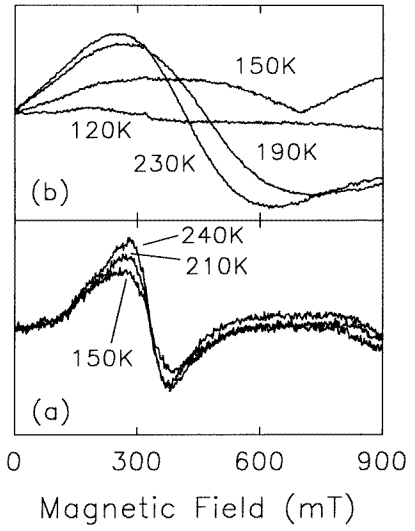

Figure 6. The temperature dependence of the EPR signal of (a) $BiPbSr_2MnO_6$ and (b) $Bi_2Sr_2MnO_{6+x}$ with metamagnetic features.

with the calculated x_{EPR} fraction of Mn^{3+} sites substituted by Mn^{2+} ions. Two facts may be pointed out: (i) it seems that, above a critical x_{EPR} value of about 0.5, the number of EPR-active sites (that is the number of substituted Mn^{3+} ions) inhibits the long-range magnetic ordering, and paramagnetic phases are observed (e.g. sample C); (ii) below this value, metamagnetic or AF behaviour is observed, arising from ferrimagnetism within the MnO_2 planes (according to the model in [10]). In particular, metamagnetic properties are detected in samples with not too low concentration of substitutional Mn^{2+} ions (sample B). Let us now comment on these points in more detail.

The lack of magnetic ordering in (i) appears similar to the effect of diamagnetic dilution of magnetic oxides above a critical value of concentration of substitutional diamagnetic ions, but Mn^{2+} ions possess non-null magnetic moment as well as the substituted Mn^{3+} ions. In our case, the relevant difference between Mn^{3+} sites and Mn^{2+} sites is the ionic magnetic anisotropy. The anisotropic and large zero-field splitting of the Mn^{3+} ion gives rise to a system with $g_z \gg g_x = g_y$, that is with low spin dimensionality approaching the Ising magnetic model. By contrast, Mn^{2+} ions quite closely approximate the isotropic Heisenberg model with three-dimensional (3D) spin features. The different spin dimensionality can crucially determine the real occurrence of long-range magnetic order at finite temperature in a magnetic structure with low lattice dimensionality, such as that of these layered oxides. As a matter of fact, since the out-of-plane exchange interactions are negligible with respect to the AF interactions within the MnO_2 layers [10], the magnetic structure may be considered as a 2D system. In this case, it was proved that Heisenberg systems cannot sustain long-range magnetic order at any non-zero temperature [18] while Ising systems can. Thus, substitution of strongly anisotropic Mn^{3+} spins with nearly isotropic Mn^{2+} spins in a layered magnetic structure may really mean frustration of the long-range magnetic ordering, up to its complete disappearance.

Let us now discuss point (ii). The coexistence of cations with different magnetic moments is clearly not sufficient to determine ferrimagnetic order. In fact, cationic

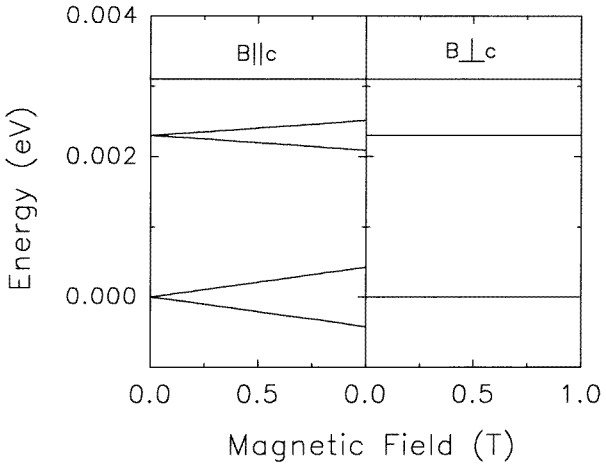

Figure 7. The energy level structure of the low-energy multiplet of Mn^{3+} with the magnetic field along the *c* axis and orthogonal to the *c* axis.

substitution with different magnetic ions in magnetic materials often results in the mere change of the mean magnetic moment of the magnetic lattice(s), provided that the substitutional ions participate in the magnetic order. Therefore, the ferrimagnetic moment observed in our samples, and in single crystals [10], should be the fingerprint of the occurrence of two factors: first, Mn^{2+} ions should take part in the magnetic ordering, as evidenced by their contributions to the spontaneous magnetization of the layers; second, Mn^{2+} ions are not randomly distributed, but substitute preferentially distinct non-equivalent cationic sites among the three [10] crystallographically different manganese sites within the modulated structure of $Bi_2Sr_2MnO_{6+x}$. In fact, ferrimagnetism implies some kind of distinction between the cationic sites occupied by each species of magnetic ion so as to give rise to uncompensated antiferromagnetically coupled sublattices. This condition can be easily encountered in $Bi_2Sr_2MnO_{6+x}$ where the AF structure is constituted by *two* magnetic sublattices of antiparallel spins shared among *three* distinct lattice sites arising from the structural modulation. Therefore, ferrimagnetic layers can arise from the coexistence of different manganese spin states and the particular structural deformation. The weak interactions between MnO_2 layers along the *c* axis should favour the ordering of the ferrimagnetic layers in AF structures [10] for low magnetic fields. Our data (see table 1) suggest that the observation of field-induced transitions to 3D ferrimagnetic order (sample B), also detected in single crystals [10], is crucially related to the presence of a relevant concentration of Mn^{2+}, since AF behaviours are observed in samples with Mn^{2+}–Mn^{3+} ratio lower than about 0.4 (sample D).

Finally, let us now comment the role of the deviations of the Mn formal valence in $BiPbSr_2MnO_6$. In this compound, lacking the structural modulation peculiar to the samples without Pb, the remanent magnetization observed in single crystals [13] was interpreted as weak ferromagnetism due to in-plane anisotropy, whose origin remained unknown. On the other hand, the lack of net magnetic moment in our lead-free sample suggests that the weak ferromagnetic features observed in [13] were critically affected by some sample-dependent parameters, such as the oxygen content, which may change the Mn oxidation state. Indeed, the lack of remanent magnetization in our sample is accompanied by the lowest concentration of EPR centres in our set of samples. This result puts forward a crucial

role of the substitutional Mn^{2+} ions in determining weak ferromagnetism, and confirms the stoichiometricity of the composition obtained. In fact, the effect of the oxygen has already been checked [13], demonstrating the occurrence of remanent magnetization in oxygen-annealed samples. Once more, it should be considered that variations of the oxygen content may induce different Mn configurations as well as structural deviations.

5. Summary

EPR and χ data suggest we consider the presence of different Mn valence states as responsible, together with the structural features, for the variety of magnetic properties observed in $Bi_2Sr_2MnO_{6+x}$ and $BiPbSr_2MnO_6$. Comparison between χ and EPR data within a set of differently prepared $Bi_2Sr_2MnO_{6+x}$ samples suggests that the Mn^{2+}-substituted Mn^{3+} sites may constitute nearly isotropic magnetic sites frustrating the 2D AF structure sustained by Ising-like Mn^{3+} spins. In-plane ferrimagnetism would arise from segregation of different Mn spin states among distinct structural sites, while the inter-plane order would be ferromagnetic or AF as a function of the amount of Mn^{2+} ions. Similarly, the lack of weak ferromagnetism in stoichiometric $BiPbSr_2MnO_6$ suggests that Mn^{2+} is responsible for the behaviour observed in single crystals [10].

References

[1] Di Stasio M, Müller K A and Pietronero L 1990 *Phys. Rev. Lett.* **64** 2827
[2] Anderson P W 1987 *Science* **235** 1196
[3] Baskaran G 1987 *Physica* B **148** 200
[4] Sunshine S A *et al* 1988 *Phys. Rev.* B **38** 893
[5] Tarascon J M, LePage Y, Barboux P, Bagley B G, Greene L H, McKinnon W R, Hull G W, Giroud M and Hwang D W 1988 *Phys. Rev.* B **37** 9382
[6] Bowden G J, Elliston P R, Wan K T, Dou S X, Easterling K E, Bourdillon A, Sorrell C C, Cornell B A and Separovic S 1987 *J. Phys. C: Solid State Phys.* **20** L545
[7] Simon P, Bassat J M, Oseroff S B, Fisk Z, Cheong S-W, Wattiaux A and Schultz S 1993 *Phys. Rev.* B **48** 4216
[8] Tarascon J M *et al* 1989 *Phys. Rev.* B **39** 11587
[9] LePage Y, McKinnon W R, Tarascon J M and Barboux P 1989 *Phys. Rev.* B **40** 6810
[10] McKinnon W R *et al* 1991 *Phys. Rev.* B **41** 4489
[11] Catti M, Dalba G, Fornasini P and Mölgg M 1994 *J. Solid State Chem.* **112** 392
[12] Levy D, Fu W T, Ijdo D J W and Catti M 1994 *Solid State Commun.* **92** 659
[13] McKinnon W R, Tselepis E, Tarascon J M, Miceli P F, Remschnig K and Hull G W 1991 *Phys. Rev.* B **43** 5468
[14] Selwood P W 1956 *Magnetochemistry* (New York: Interscience) p 78
[15] Abragam A and Bleaney B 1970 *Electron Paramagnetic Resonance of Transition Ions* (New York: Oxford University Press) p 434
Landolt–Börnstein *New Series* 1979 vol 10 (Berlin: Springer) p 836
[16] Gerritsen H J and Sabiski E S 1963 *Phys. Rev.* **132** 1507
[17] See, for example, Hutchings M T 1965 *Solid State Physics* vol 16 ed F Seitz and D Turnbull (New York: Academic) p 227
[18] De Jongh L J 1990 *Magnetic Properties of Layered Transition Metal Compounds* (Dordrecht: Kluwer) p 10